RESEARCH PAPER

Quantitative Insight into the Compressive Strain Rate Sensitivity of Polylactic Acid, Acrylonitrile Butadiene Styrene, Polyamide 12, and Polypropylene in Material Extrusion Additive Manufacturing

N. Vidakis[1] · M. Petousis[1] · I. Ntintakis[1] · C. David[2] · D. Sagris[2] · N. Mountakis[1] · A. Moutsopoulou[1]

Abstract

Herein, a research and engineering gap, i.e., the quantitative determination of the effects of the compressive loading rate on the engineering response of the most popular polymers in Material Extrusion (MEX) Additive Manufacturing (AM) is successfully filled out. PLA (Polylactic Acid), ABS (Acrylonitrile Butadiene Styrene), PP (Polypropylene), and PA12 (Polyamide 12) raw powders were evaluated and melt-extruded to produce fully documented filaments for 3D printing. Compressive specimens after the ASTM-D695 standard were then fabricated with MEX AM. The compressive tests were carried out in pure quasi-static conditions of the test standard (1.3 mm/min) and in accelerated loading rates of 50, 100, 150, and 200 mm/min respectively per polymer. The experimental and evaluation course proved differences in engineering responses among different polymers, in terms of compressive strength, elasticity modulus, toughness, and strain rate sensitivity index. A common finding was that the increase in the strain rate increased the mechanical response of the polymeric parts. The increase in the compressive strength reached 25% between the lowest and the highest strain rates the parts were tested for most polymers. Remarkable variations of deformation and fracture modes were also observed and documented. The current research yielded results with valuable predictive capacity for modeling and engineering modeling, which hold engineering and industrial merit.

Keywords Fused filament fabrication · Additive manufacturing · Melt Extrusion · Compressive strain rate sensitivity · Engineering response

✉ N. Vidakis
    vidakis@hmu.gr

    M. Petousis
    markospetousis@hmu.gr

    I. Ntintakis
    ntintakis@hmu.gr

    C. David
    david@ihu.gr

    D. Sagris
    dsagris@ihu.gr

    N. Mountakis
    mountakis@hmu.gr

    A. Moutsopoulou
    amalia@hmu.gr

1   Department of Mechanical Engineering, Hellenic
    Mediterranean University, Heraklion 71410, Greece

2   Department of Mechanical Engineering, International
    Hellenic University, Serres Campus, Thermi 62124, Greece

Introduction

Additive Manufacturing, also known as 3D printing, indisputably marks a new era in the manufacturing industry over the last decades [1], with great prospects for both researchers and the industry [2, 3]. Transitioning from rapid prototyping to additive manufacturing has led to the achievement of new technological advantages [4]. The development of new materials geared toward industrial production has been a pivotal outcome [5]. One of the merits of additive manufacturing lies in its capacity to fabricate complex structures using a diverse range of materials, thereby necessitating an exploration of the mechanical behavior of various materials under differing loading conditions [6].

Among the explored materials for additive manufacturing, thermoplastics take a prominent place, often utilized through the Fused Filament Fabrication (FFF)

technique [7–9], which belongs to the material extrusion (MEX) family of 3D printing methods. FFF technique stands out as an economical and straightforward method for producing 3D printed components, owing to its cost-effectiveness, user-friendly nature, and expedient processing velocity [10]. This expeditious prototyping procedure finds its applicability across diverse sectors, including automotive, aerospace, medical, construction, and electrical domains [11]. Beyond conventional thermoplastic materials such as PLA (Polylactic Acid) and ABS (Acrylonitrile Butadiene Styrene) [12], novel materials have emerged in the realm of additive manufacturing. Prominently, utilized polymeric materials such as PP (Polypropylene) [13] and PA12 (Polyamide 12) [14] have emerged, contributing to the dynamic evolution of additive manufacturing.

ABS and PP are primarily petroleum-derived polymers, meaning that they are produced from petrochemical sources [15]. On the other hand, PLA and PA12 are thermoplastics made from living organisms, which means that they are characterized as bio-based polymers [16]. The increasing awareness among consumers about the environmental repercussions of petrochemical-sourced polymers has ignited interest in previously untapped sectors [17].

PLA is one of the most widely used materials in additive manufacturing [18], for various reasons such as its sustainability and eco-friendliness [19–22]. The performance of parts made by the PLA polymer has been studied and applied in a diverse range of applications [23–25]. PLA is classified as a semi-crystalline polymer, characterized by a melting temperature spanning from 170 to 180 °C [26]. Components derived from PLA exhibit a pronounced resistance to deformation [27, 28]. The behavior of PLA samples in different raster angles has been studied [29]. Compared to conventional plastics, a PLA part degraded from six months to two years [30]. As a result, PLA holds potential for applications where short-lived lifespan and biodegradability are strongly desired, such as in plastic containers [31].

ABS (Acrylonitrile Butadiene Styrene) belongs to the family of thermoplastic polymers, constituting a widely utilized member of this category [32]. ABS finds application in 3D printing, predominantly through MEX or FFF 3D printers. This prevalent thermoplastic material garners popularity owing to its suitability for desktop 3D printing and its material attributes [33]. The impact of critical process control parameters on the surface roughness, dimensional accuracy, and porosity of ABS samples have been studied already [34, 35]. Furthermore, ABS polymers exhibit remarkable resistance against various chemical compositions [36]. With a glass transition temperature of 105 °C, ABS plastic finds its suitability in applications involving relatively secure and user-friendly machinery, particularly emphasizing the significance of safety in household equipment [37]. The orientation of the raster was discovered to impact the tensile strength of ABS parts, whereas the width of the printed beads and the temperature of the bed exhibited minimal influence on this characteristic [38].

Polypropylene (PP) is the world's second most widely utilized thermoplastic due to its favorable amalgamation of robust mechanical attributes, inert characteristics, and enduring stability over extended periods [39]. It finds its applications in diverse sectors such as automotive, construction, household articles, and injection molding processes [40]. However, in AM techniques still, only a limited number of commercially accessible PP-based filaments exist [28]. PP printability is dependent on its tendency to deform during the 3D printing process [41]. Pure PP 3D printing filaments are available, as well as infused with additives such as glass fiber, talc powder, or an ethylene copolymer [42]. Of notable significance is PP's intrinsic chemical stability, rendering it impervious to a diverse array of chemical agents, encompassing acids and alkalis [40]. Additionally, polypropylene demonstrates resistance to impact-induced stress, thereby evading fracture and fragmentation [43]. Moreover, the material's robustness is evidenced by its capacity to endure a multitude of stress cycles, spanning into the millions, while maintaining structural integrity without succumbing to failure [44].

PA 12 (Polyamide 12) substantiates its position as a versatile thermoplastic, renowned for its range of additive applications [14]. The performance of parts made by the PA12 polymer has been studied [14, 45–47]. It is a prevalent material, facilitating the fabrication of utilitarian components and prototypes with functional attributes [48]. Components fabricated from PA12 exhibit notable robustness, enduring stability over prolonged temporal spans, manifesting chemical resistance, and an exceptional degree of versatility [49].

The mechanical properties of polymer parts fabricated by additive manufacturing have been studied in the literature [50–53]. Numerous research papers have addressed the examination of Fused Filament Fabrication (FFF)-processed polymers under diverse loading conditions [54–57]. A substantial number of these studies have concentrated on investigating the strain rate sensitivity exhibited by polymeric materials processed via Additive Manufacturing (AM) [58–61]. Conversely, the assessment of the behavior of polymeric AM materials through compression tests has not undergone comprehensive exploration [22, 62–66].

This present manuscript is dedicated to reporting the compression response of polymeric materials, including ABS, PLA, PP, and PA12, in the context of AM processing. Compressive loads and stresses are important in mechanical structures [67, 68]. They are common types of loadings, which are not often assessed in the literature, especially for 3D parts, probably due to the large size of the samples, which require a lot of material and time to be prepared for testing in accordance with the corresponding standard [69].

Herein, among others, the strain rate sensitivity metric during the compression experiments is also investigated. This parameter, usually denoted with the "*m*" index, is critical in dynamic loading phenomena, especially in polymeric materials. Such phenomena are common in industrial environments. The strain rate sensitivity parameter is calculated as shown in the following Eq. (1) [70–72]:

$$m = \frac{\Delta ln\,(\sigma)}{\Delta ln(\dot{\epsilon})} \tag{1}$$

The scope of the present manuscript encompasses the execution of compression tests under various structural loading conditions. Samples from the four aforementioned polymers were prepared from raw materials with a thermomechanical method (filament extrusion and 3D printing of samples with the MEX method, employing the prepared filaments). The samples were tested with test speeds varying from 1.3 to 200 mm/min $(2.16 \times 10{-}5$ s-1–$3.3 \times 10{-}3$ s−1) and their performance and behavior are presented and analyzed. The fracture mechanism in all cases was also analyzed and presented in the study. It is pertinent to note that the analysis of anisotropy in 3D-printed structures has not been undertaken in the current study. It is worth highlighting that the consideration of strain rate and compression sensitivity as design factors has previously been employed to evaluate the anisotropic characteristics of printed structures [73]. To the authors' best knowledge, no similar study exists so far for these four polymers in MEX 3D printing, reporting their mechanical performance under such loading scenarios. Herein, the experiments were not conducted with steady-state conditions only with the test speeds the standards instruct, as the literature presents so far. Higher test speeds were investigated, to investigate the effect of higher strain rates on the behavior of the specific 3D-printed polymeric materials under compression loads. No similar study, to the authors' best knowledge, addresses this subject in the literature so far for these polymeric materials. The effect of high strain rates under compression loads has been presented for other polymeric materials in 3D printing, i.e., Polycarbonate (PC), Polyethylene terephthalate glycol (PETG), Polymethyl methacrylate (PMMA), and Thermoplastic polyurethane (TPU) [74]. The results of the study can be directly exploited in industrial environments for the design of parts to be built with these four popular polymers with the MEX 3D printing process.

Materials and Methods

Materials for Extrusion

Five specimens of each polymer, i.e., Polylactic acid (PLA), Acrylonitrile Butadiene Styrene (ABS), Polypropylene (PP), and Polyamide 12 (PA12) were fabricated by using the material extrusion (MEX) 3D printing technique. Specifically, the raw materials were procured as follows: PLA thermoplastic, from Plastika Kritis SA of Heraklion, Crete, Greece, ABS from INEOS Styrolution (INEOS Styrolution Group GmbH, Frankfurt, Germany), PP from JULIER (Fujian, China) and PA12 by Arkema S.A. of Colombes, France.

Methods

The flowchart diagram (Fig. 1) shows the methodological approach used. The process starts from the raw material preparation to the subsequent filament fabrication process, continuing with the execution of compression tests as presented in Fig. 1. Each of these sequential stages is expounded upon in a comprehensive manner within the subsequent sections.

Filament Preparation and Extrusion

The filament fabrication started with a drying procedure of the raw materials within well-defined and meticulously regulated conditions. Then the extrusion of filaments follows, using the 3D Evo Composer 450 desktop extruder (3D Evo, Utrecht, The Netherlands). The filament's nominal diameter was set to 1.75 mm. The acceptable tolerance was ± 0.07 mm. The filament's diameter was controlled via an integrated optical sensor. The raw material traverses a sequence of four distinct heating zones during the extrusion process in the extruder chamber. The temperatures within these heating zones necessitate meticulous control, contingent upon the intrinsic properties of the polymer material. The extrusion specifications pertinent to each polymer material are presented in Table 1. Post-extrusion, the filament's diameter, and surface roughness were checked for assessment and verification.
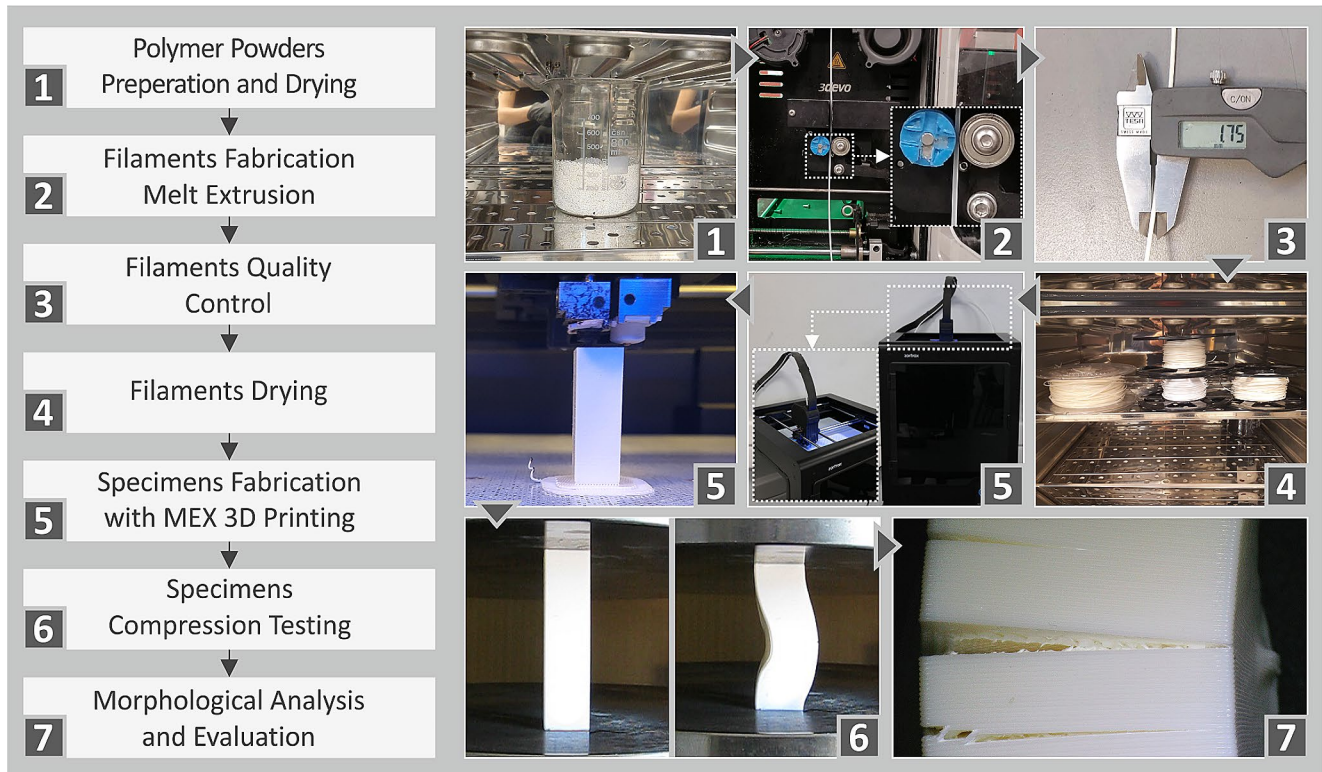
Fig. 1 The methodological flowchart encapsulates distinct phases, starting from the preparation of specimens, progressing through the extrusion process, the fabrication phase, and the subsequent testing procedure. On the right-side images from the experimental steps conducted are depicted

Table 1 Extrusion specifications for all four polymer materials during filament fabrication

	PLA	ABS	PP	PA12
Heat Zone 1 (°C) (nozzle)	195	190	195	210
Heat Zone 2 (°C)	205	230	205	220
Heat Zone 3 (°C)	205	240	205	220
Heat Zone 4 (°C) (hopper)	175	220	195	185
Rotation Speed of screw (rpm)	8.5	5	3	8.5
Rotational speed of winder (rpm)	3–15	3–15	3–15	3–15

Table 2 3D printing settings for the fabrication of the specimens

	PLA	ABS	PP	PA 12
Print Speed (mm/s)	70	40	40	40
Extrusion Temperature (°C)	210	260	250	270
Bed Temperature (°C)	50	90	110	90

specimens. Determining optimal 3D printing settings for each polymer material necessitated a preliminary preparatory experimental procedure. Table 2 shows the setting of 3D printing of each polymer material.

Fabrication of Compression Specimens

The additively manufactured compression test specimens were fabricated according to the American Society for Testing and Materials (ASTM) D695-02a standard. For each distinct material, a series of five samples (prismatic, measuring 12.7 mm × 12.7 mm × 25.4 mm) per strain rate (overall one hundred samples), were fabricated with the Fused Filament Fabrication (FFF) technique using the Intamsys Funmat HT 3D printer (Shanghai, China). All filaments were dried for four hours at a temperature of 50 °C. For consistency, a uniform infill density of 100% was applied to all specimens, while a nozzle featuring a diameter of 0.4 mm was universally employed in the fabrication of these specimens. Similarly, the 3D printing orientation and direction remained consistent for all

Testing Procedure

The Instron KN1200 (Norwood, Massachusetts, United States) device was used for the compression tests. To evaluate the behavior of each polymer under different conditions the compression speed varied from 1.3 to 200 mm/min. In particular, the tested speeds were 1.3, 50, 100, 150, and 200 mm/min (2.16×10^{-5} s^{-1} – 3.3×10^{-3} s^{-1}) to cover a broad range of compression rates in working conditions. For each polymer five specimens have been evaluated at constant room temperature in each different testing speed scenario. All tests were conducted in ambient room conditions (23 °C temperature, 55% humidity). The compression properties were calculated from the

experimental data. The yield stress was determined by applying the 0.2% offset method [75].

Raman Spectra, Thermal and Rheological Properties Evaluation for the Four Polymers Tested

The polymeric materials were subjected to thermogravimetric analysis (TGA) (PerkinElmer Diamond, Waltham, USA, 10 °C per minute rate, from room temperature to up to 550 °C). To further assess the thermal properties of the specific polymeric raw materials tested, Differential Scanning Calorimetry (DSC) was also carried out (TA-Instruments, DSC-25 Discovery Series, New Castle, Delaware, USA, 15 °C/min step, heating cycle 25–300–25 °C).

Raman spectra were acquired on a modified LabRAM-HR Spectrometer, by HORIBA Scientific in Kyoto, Japan. An optimal wavelength of 532 nm using a solid-state laser module with an ultimate generated power of 90 mW, was used for excitation. The illumination of the sample was made with excitation light. The resulting Raman signals were gathered using an Olympus LMPlanFL-N 50× microscopic objective lens with a numerical aperture of 0.5 and an operating distance of 10.6 mm. To reduce the power, a Neutral Density filter with 1% transmittance was employed, resulting in a measured power of 400 μW on the specimen. The laser beam's focal spot measured approximately 1.70 μm laterally and around 2.0 μm along the axis. A spectral resolution of approximately 2.0 cm^{-1} was achieved using a 600-groove grating. The Raman spectral range spanned from 50 to 3900 cm^{-1}, and three optical windows covered each measurement point. Each measurement point was subjected to an acquisition time of 10 s with 5 accumulations.

The rheological properties were evaluated using a Discovery Hybrid Rotational Rheometer DHR-20, manufactured by TA-Instruments. This instrument was outfitted with two parallel plates and an Environmental Test Chamber, ensuring precise temperature control for the analysis of rheological attributes. The measurements were conducted continuously above the melting point of the composites to maintain their fluidity. Each data point was recorded over a 10-second duration to prevent overheating of the sample. This approach safeguarded the sample's structural integrity while allowing for the collection of precise data for the rheological analysis.

Rotational rheometry tests were integrated with Melt Flow Rate (MFR) measurements to evaluate the flow properties of the materials under specific temperature and pressure conditions. This procedure adhered to the established international standard ASTM D1238-13, which outlines the testing protocol for Melt Flow Rate (MFR).

The MFR measurement unveiled the material's melt viscosity and flow behavior.

Results & Discussion

Assessment of the Thermal, Structural, and Rheological Characteristics of the Four Polymers Tested

TGA graphs for the four polymeric materials assessed are depicted in Fig. 2. TGA analysis was conducted to confirm that degradation temperatures were at least 100 °C greater than processing temperatures for the four polymers. For completeness, the thermal properties of the polymers were further assessed with DSC with the results shown in Fig. 3b. As depicted in Fig. 3b, there are differences in the phase change temperatures between the polymers and the absorbed energy during the test.

The Raman spectra for each one of the four polymers are presented in Fig. 3a. The acquired peaks were checked against the published literature. In the supplementary material of the study, a table is provided for each polymer with the corresponding literature documentation to support the findings. Viscosity and stress vs. shear rate graphs for each polymer, as they were determined by the rheology tests are presented in Fig. 3c. The rheology differs between the polymers. ABS has the highest viscosity, then PLA, then PP, and PA12 showed the lowest viscosity values. Figure 3d shows the corresponding MFR values derived from the rheological tests. ABS has the lowest MFR, and the PP polymer has the highest one, almost an order of magnitude higher than ABS. Such differences justify the different 3D printing conditions required to 3D print parts with each polymer.

Compression Results of the PLA Polymer

Figure 4a illustrates the stress-strain curves under compression at various speeds: 1.3, 50, 150, and 200 mm/min. Notably, at 200 mm/min, the PLA sample demonstrates higher performance, surpassing 25 MPa. It closely parallels the performance of the 150 mm/min sample. The performance at 100 mm/min is almost 25 MPa. Figure 4b shows the compressive strength of PLA polymers across each compression speed. The highest strength (sb) occurs at 200 mm/min, while the yield strength (sY) is greater for a compression speed of 150 mm/min. The compression Modulus of Elasticity for each compression speed is detailed in Fig. 4c. At 200 mm/min, the PLA polymer's modulus of elasticity spans from 1.5 to 1.8 GPa, with an average value of 1.75 GPa. For a compression speed of
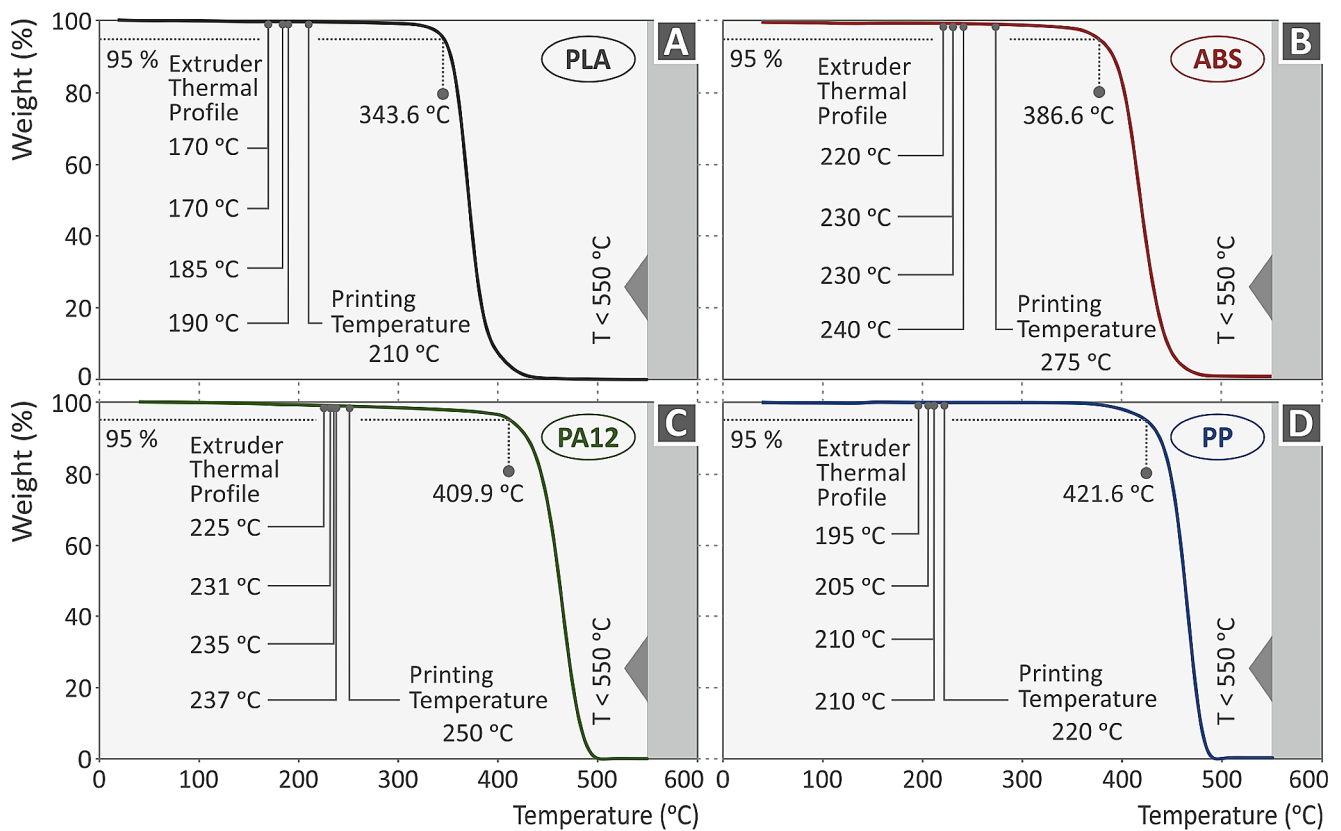
Fig. 2 3D printing and extrusion temperatures for each polymeric material studied herein correlated with the respective thermal degradation response, as it was derived during the experimental procedure with thermogravimetric analysis (TGA)

150 mm/min, the average value is 1.65 GPa, while for 100 mm/min, it exceeds 1.65 GPa. Figure 4d presents the computed compression sensitivity index (m) in relation to the corresponding compression values (%) for varying loading conditions.

Compression Results of the ABS Polymer

The stress-strain curves corresponding to compression speeds of 1.3, 50, 100, 150, and 200 mm/min of 3D-printed specimens made with the ABS polymer are illustrated in Fig. 5a. Notably, the highest compressive strength is observed at 200 mm/min, while the lowest one is witnessed at 1.3 mm/min. Figure 5b presents the compressive strength across distinct compression speeds. The results show that the highest sB occurs at a compression speed of 200 mm/min, while the sY is greater at 150 mm/min. The compression Modulus of Elasticity is relatively consistent for compression speeds of 50 and 100 mm/min, both exceeding 1.8 GPa. The maximum value is recorded at 200 mm/min, over 1.9 GPa, as depicted in Fig. 5c. Figure 5d provides insight into the computed

compression sensitivity index (m) in relation to the corresponding compression values (%) for diverse loading conditions.

Compression Results of PP Polymer

Figure 6 illustrates the results of compressive testing on 3D-printed specimens made with the PP polymer. The data reveals similar compressive stress values (in MPa) for compression speeds of 50 and 150 mm/min (Fig. 6a). The higher compressive stress was found at 200 mm/min. The sB was higher for the 200 mm/min speed value, while the sY value was higher at 150 mm/min. Comparatively, the outcomes for 100 mm/min and 150 mm/min speeds are almost similar (Fig. 6b). Concerning the compression modulus of elasticity, a higher value (0.33 GPa) was observed at the compression speed of 200 mm/min (Fig. 6c). The sensitivity index (m), relative to the corresponding compression values (%), under various loading conditions, is illustrated in Fig. 6d.
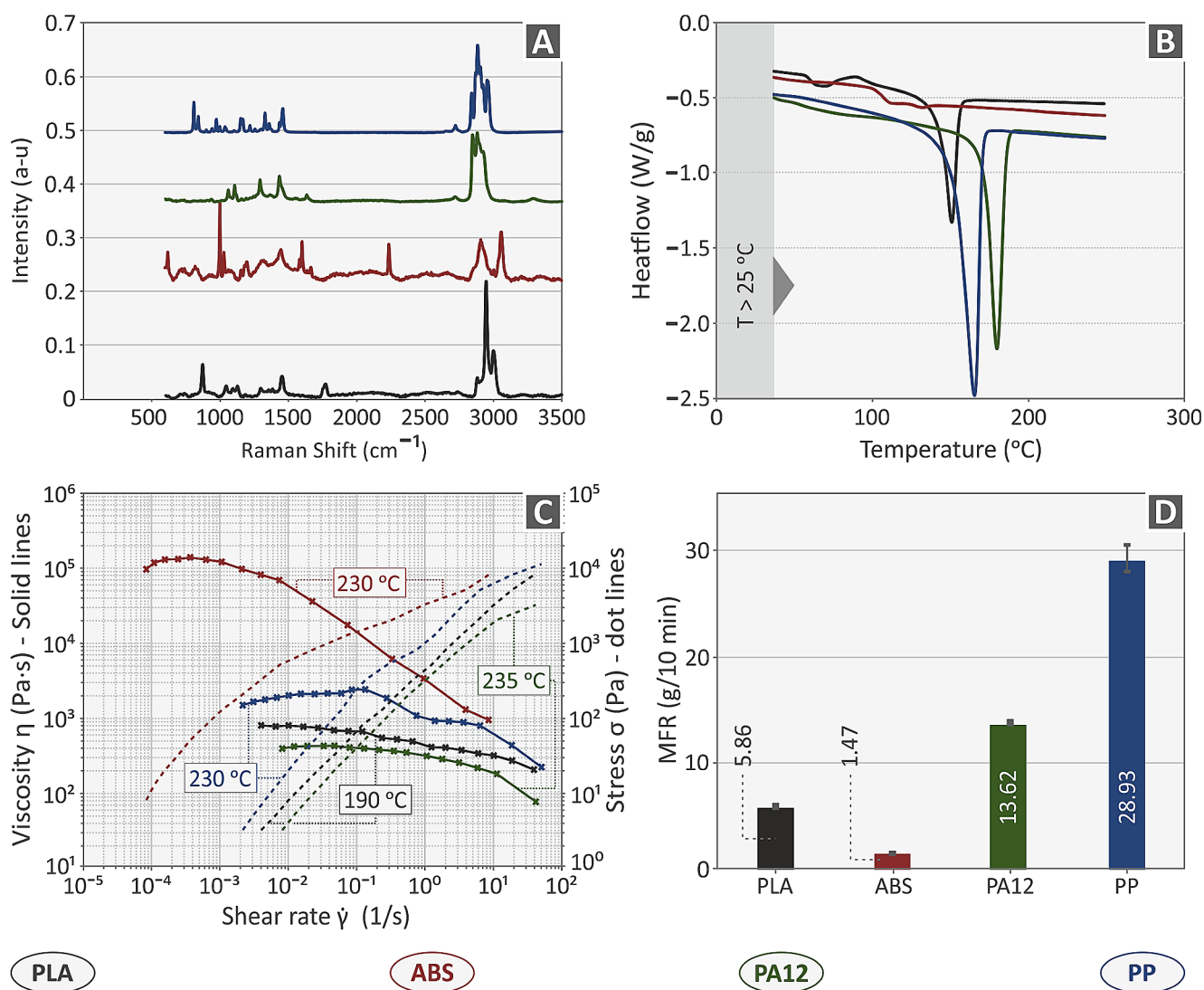
Fig. 3 For the four polymers tested (A) Raman spectra, (B) DSC graphs, (C) rheological properties, and (D) MFR

Compression Results of PA12 Polymer

Figure 7a shows the results of compression stress-strain curves for 1.3, 50, 100, 150, and 200 mm/min compression speed. From the results, the highest compressive stress (more than 50 MPa) was observed at 150 mm/min. For 200 mm/min compression speed, the stress is about 20 MPa. The result of compressive strength shows the sB and sY are higher for 150 mm/min compression speed (Fig. 7b). Figure 7c shows that the highest compression modulus of elasticity for PA 12 polymer was observed at 200 mm/min. Figure 7d shows the calculated compression sensitivity index (m) concerning the corresponding compress values (%) for different loading conditions.

Compressive Strength of the Samples

Figure 8 presents the individual behavior of each one of the four polymers to withstand static compression loads across varied compression rate loading scenarios. In Fig. 8a, the maximum compressive strength is shown, while Fig. 8b exhibits the maximum compressive yield stress. Additionally, Fig. 8c illustrates the compressive modulus under various strain rates (s^{-1}).

Compressive Toughness and Strain Rate Sensitivity of the Samples

The calculated toughness of each polymer for all compression speeds is shown in Fig. 9a. From the results, the toughness of ABS is much higher than the other three polymers, with PP having a lower value. PLA and PA12
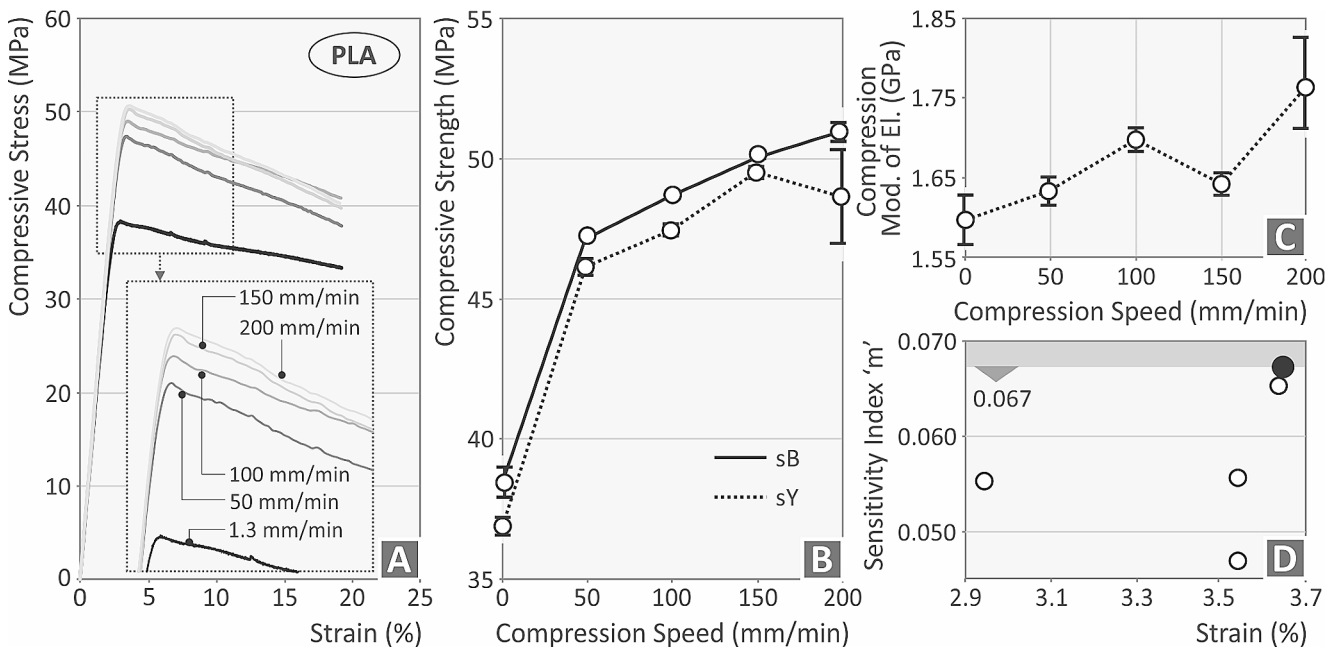
Fig. 4 (a) Compression stress—strain (MPa-%) curve of PLA polymer at 1.3, 50, 100, 150, and 200 mm/min compression speed, (b) compression strength for PLA polymer (c) compressive modulus of PLA polymer, and (d) index m—strain (%) graph for PLA polymer. The grey bar depicts the maximum sensitivity index reported for the PLA polymer. The value is presented with a different color as well
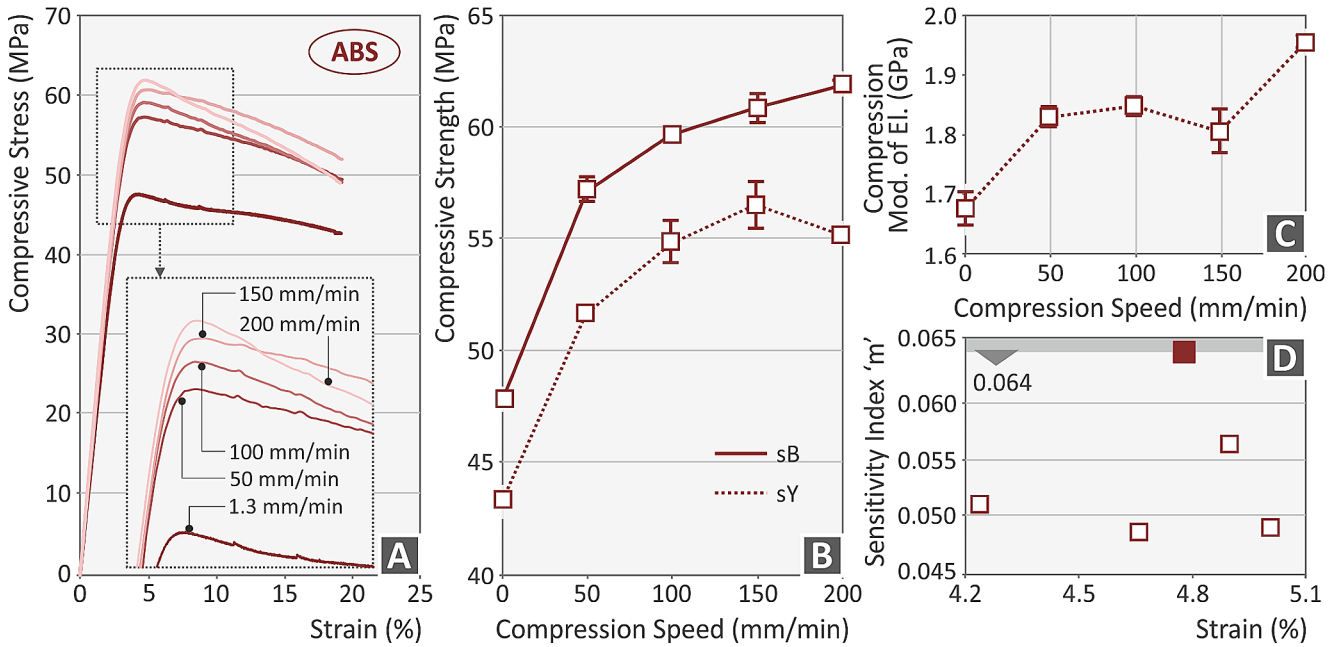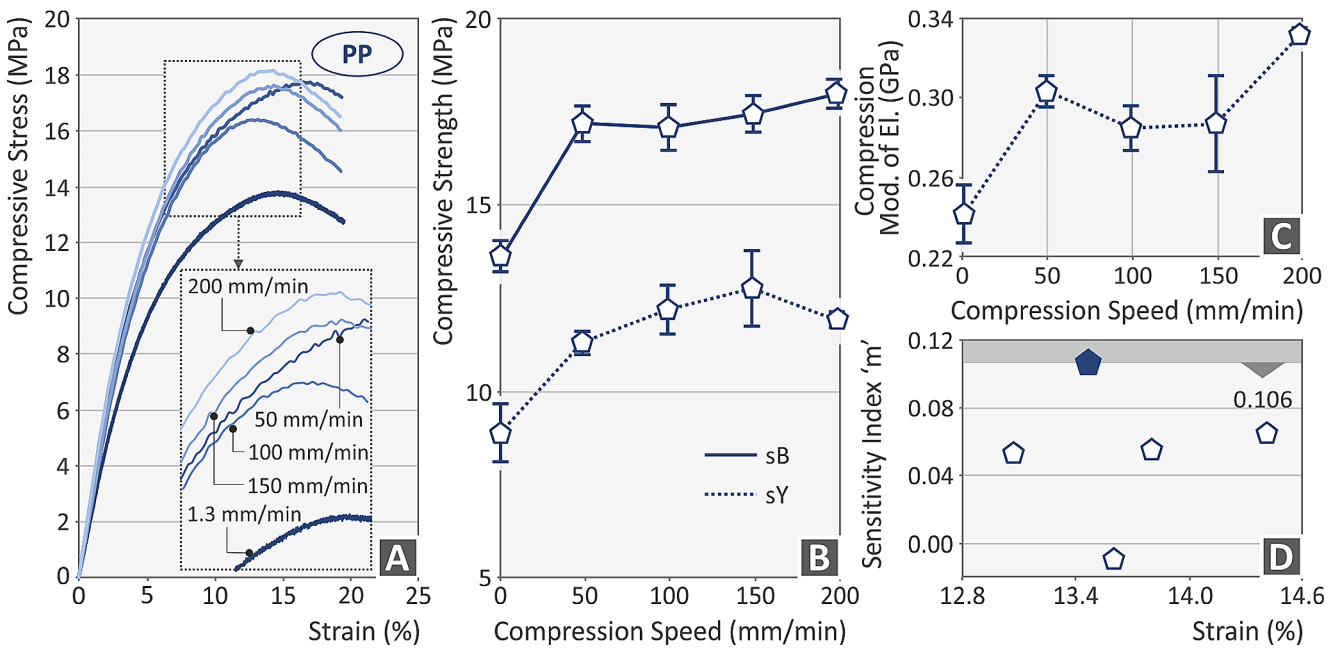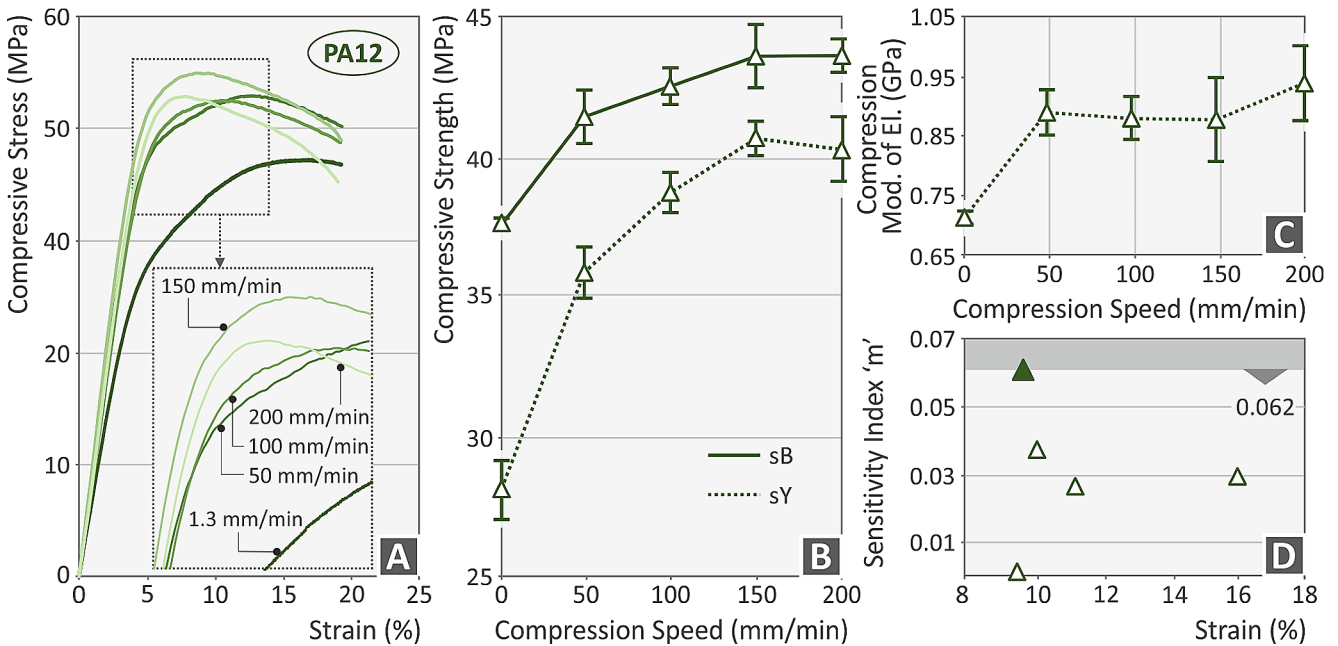

Fig. 5 (A) Compression stress—strain (MPa-%) curve of ABS polymer at 1.3, 50, 100, 150, and 200 mm/min compression speed, (B) compression strength for ABS polymer (C) compressive modulus of ABS polymer, and (D) index m—strain (%) graph for ABS polymer

Fig. 6 (A) Compression stress—strain (MPa-%) curve of PP polymer at 1.3, 50, 100, 150, and 200 mm/min compression speed, (B) compression strength for PP polymer (C) compressive modulus of PP polymer, and (D) index m—strain (%) graph for PP polymer

Fig. 7 (A) Compression stress—strain (MPa-%) curve of PA12 polymer at 1.3, 50, 100, 150, and 200 mm/min compression speed, (B) compression strength for PA12 polymer (C) compressive modulus of PA 12 polymer, and (D) index m—strain (%) graph for PA12 polymer

polymers seem to have a similar value of compressive toughness. Figure 9b presents the found compression index "m" to the maximum strain (%) observed to fracture. The PP polymer is a highly dependent polymer on the strain rate (highest strain rate sensitivity index). On the other hand, the PA12 polymer has a lower dependence of 'm' on strain rate.

Samples Morphological Characteristics

Figure 10 refers to the behavior of the PLA polymer under various compression loading speeds. At a compression speed of 1.3 mm/min, overhangs emerged along the full sample length, subsequently. They were confined to the central section (Fig. 10a). With an increased compression
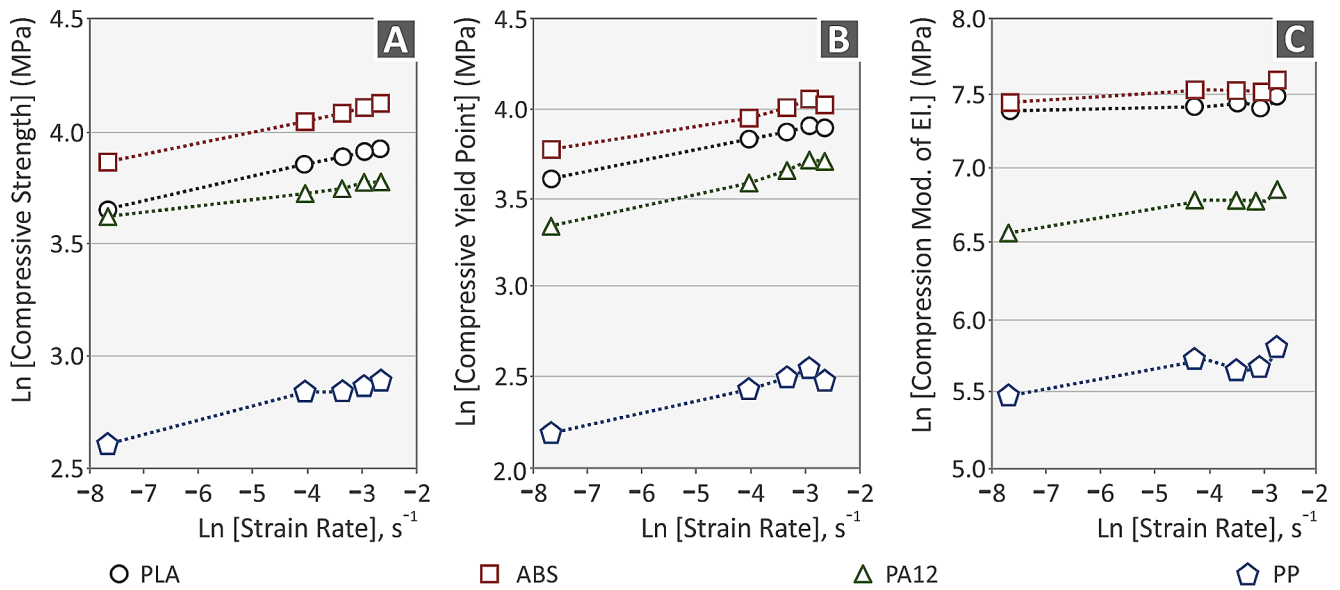
Fig. 8 (a) compressive strength to strain rate, for all four materials (b) compressive yield point (MPa), and (c) compression modulus of elasticity (MPa) (all graphs with logarithmic scale axis)
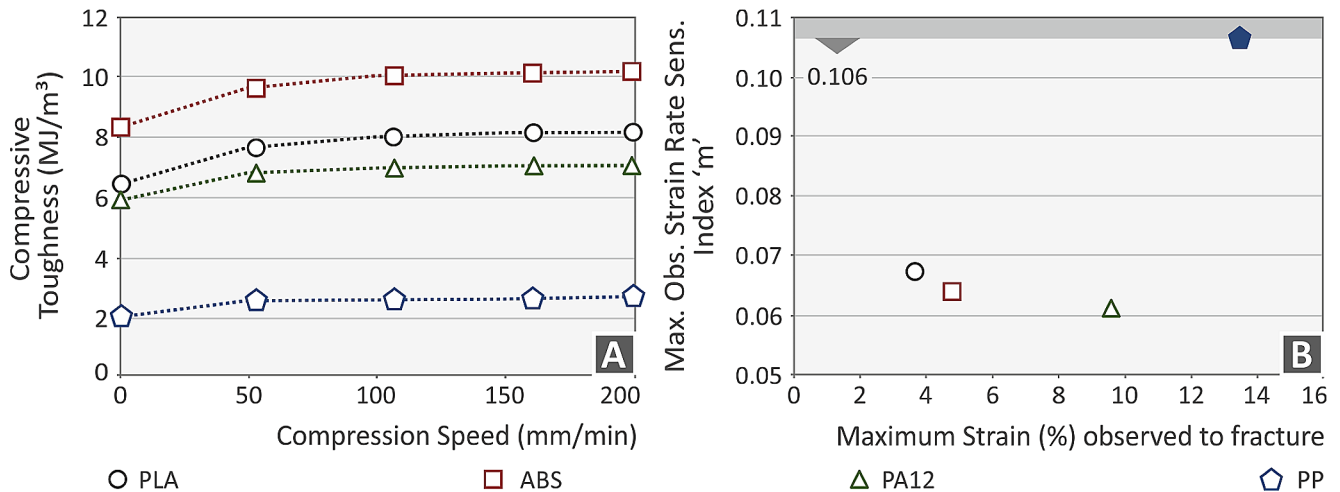

Fig. 9 (a) Compressive toughness vs. the compression speed for PLA, ABS, PP, and PA12 polymers, and (b) maximum observed index m vs. the maximum strain observed at the fracture of the specimen for all four tested polymers

speed of 50 mm/min, overhangs become more pronounced and closer to the middle height (Fig. 10b). Figure 10c shows the sample behavior under a compression speed of 100 mm/min, revealing substantial deformation. The deformation of the specimen under a compression speed of 150 mm/min is demonstrated in Fig. 10d, where overhangs were evident at the middle specimen height. Figure 10e displays the deformation of the sample at 200 mm/min, indicating the presence of cracks at the top and bottom areas. For the remaining materials, the corresponding compression test experiment images at various strain rates are shown in Figs. 11, 12 and 13 respectively. Differences can be observed in the response of the samples, related to the deformation of the samples (shape) in

the different test speeds and the formation of cracks at the failed sample. For example, the ABS deforms with the specimens forming a "C" shape, while the PA12 specimens form an "S" shape. Additionally, the ABS samples developed cracks that are evident in all test speeds, while the PA12 samples have high cracks at the highest speeds tested (150 and 200 mm/min, at 100 mm/min a very small crack is developed, Fig. 11C). No cracks are visible in the PP samples even at 200 mm/min speed of testing. The remaining (plastic) deformation in the PP samples after the completion of the experiment is also reduced compared to the other three polymers. It should be noted that, due to the 3D printing structure of the samples, differences were expected between the samples. Still, the
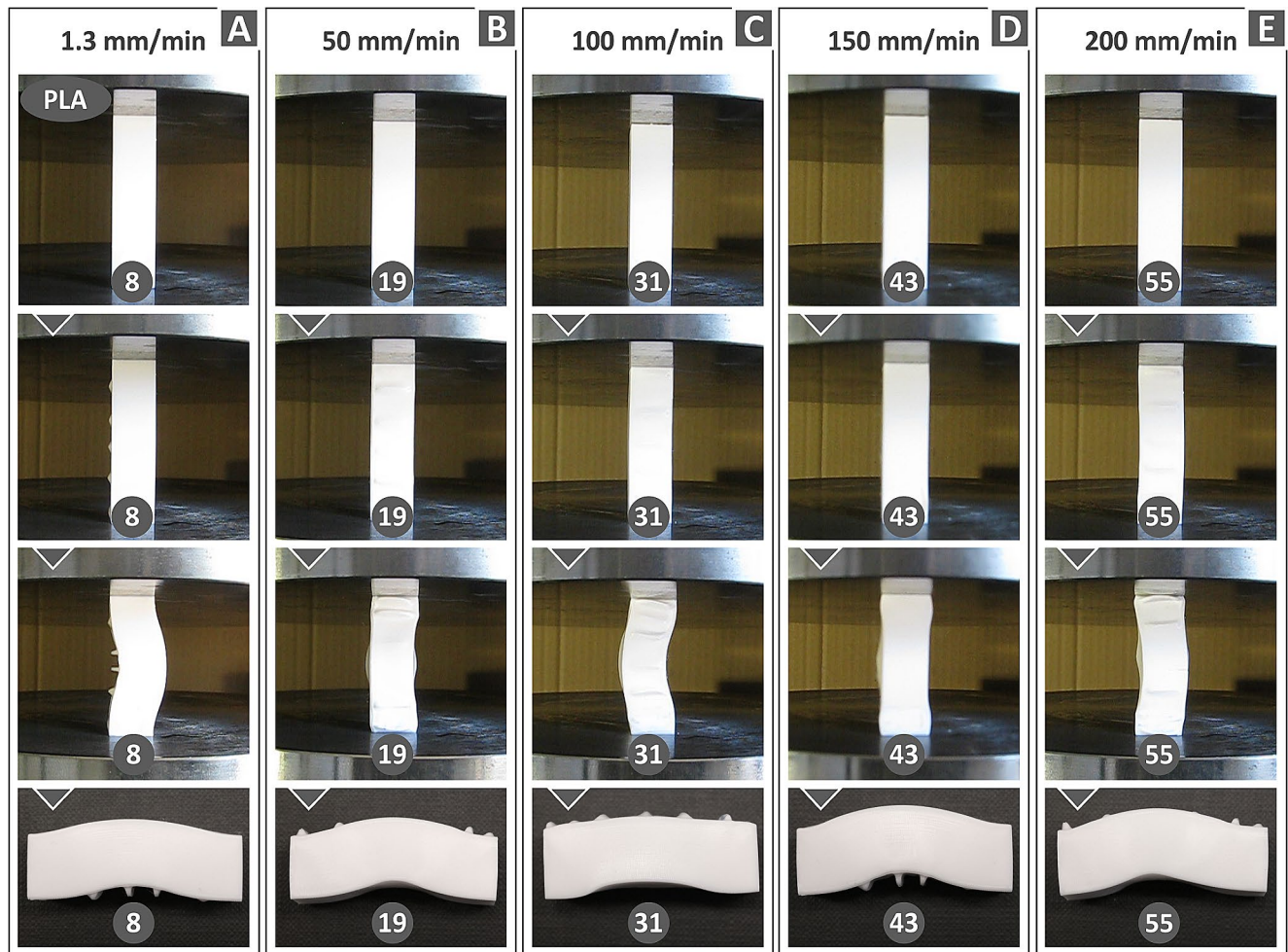
Fig. 10 PLA polymer specimens' deformation at different compression speeds, a) at 1.3 mm/min, (b) at 50 mm/min, (c) at 100 mm/min, (d) at 150 mm/min, and (e) at 200 mm/min. The specimens were numbered in the study, and the number of each specimen is depicted in each picture

deformation shapes were consistent across the replicates in each loading scenario studied.

Morphological analysis of the specimens was conducted using optical microscopy (Kern OKO 1, Albstadt, Germany). Figure 14 provides the morphological features at compression speeds of 1.3, 100, and 200 mm/min for all four polymers. For PLA at 1.3 mm/min, initial overhangs appear on the outer surface of the sample (Fig. 14a). At a compression speed of 100 mm/min, larger overhangs are observed on the outer surface. When the compression speed is set to 200 mm/min, a crack appears without affecting the entire sample width. Initial cracks are noticeable on the inner surface of the ABS sample at 1.3 mm/min (Fig. 14b). These cracks expand for compression speeds of 100 mm/min and 200 mm/min. Similar trends are seen in the PA12 sample, with an initial crack at 1.3 mm/min that enlarges at 100 mm/min and leads to fracture at 200 mm/min (Fig. 14c). In contrast, the behavior of the PP sample (Fig. 14d) displays

no cracks across all compression speeds (1.3, 100, and 200 mm/min), showcasing superior performance relative to the other polymers.

Discussion

Polymers exhibit viscoelastic properties, and their mechanical response is highly sensitive to both the rate at which an external mechanical load is applied and the temperature of the surrounding environment, referred to as operational temperature [72, 76, 77]. This was verified in the study, with the increase in the compressive strength of all four polymers with the increase of the strain rate applied during the experimental procedure. The temperature was kept constant throughout the experiments, as mentioned above. At low strain rates strain hardening phenomena in polymers exist but are barely present [78]. However, polymeric chains can potentially undergo some
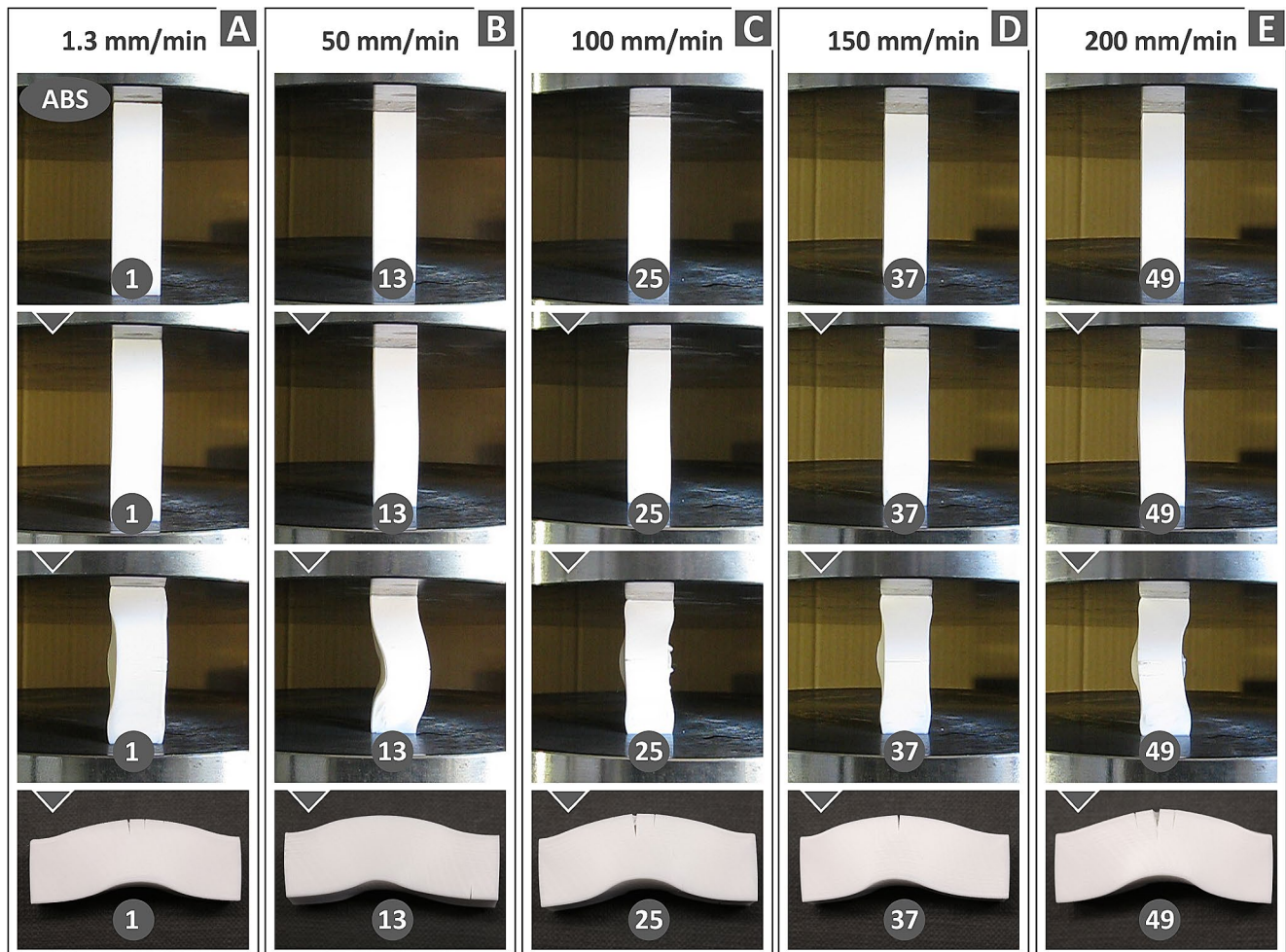
Fig. 11 ABS polymer specimens' deformation at different compression speeds, a) at 1.3 mm/min, (b) at 50 mm/min, (c) at 100 mm/min, (d) at 150 mm/min, and (e) at 200 mm/min

degree of alignment or orientation, resulting in enhanced toughness. This orientation contributes to the material's ability to resist deformation more effectively and carry heavier loads [72, 79, 80]. Furthermore, different types of polymers can exhibit varying degrees of strain hardening, leading to increased toughness [72, 81–83]. This was also verified in the study and is directly related to the strain rate sensitivity index "m", which was calculated for all polymers tested. As shown the PP polymer had a higher strain rate sensitivity index "m" than the other three polymers, which had similar values for this index. While polymers are commonly used in applications with low loads, the rate at which the load is applied can even lead to a "catastrophic fracture," underscoring the importance of considering parameters, such as the strain rate sensitivity index "m" in material selection. Herein, 3D printing structures were examined, which have different mechanical behavior than the bulk materials. As the "m" metric increases, it shows that the specific polymer is

more sensitive to strain rate changes, and it is reported herein that the PP polymer is the most sensitive one among the four polymers studied. For the PLA and the ABS polymer, this scattering in the "m" metric values is lower. The "m" values between the lower and the higher strain rates differ by about 25% in these two polymers.

The observed buckling in the specimens examined diverges from the conventional Euler elastic buckling observed in bulk materials, where it is contingent upon the material's stiffness and the geometric shape of the specimen. In the case under consideration, the specimens, structured through the FFF method, exhibit layering and anisotropy. Consequently, when subjected to longitudinal compression loading, the structure experiences collapse induced by shear stresses, leading to the formation of shear bands. These shear bands undergo slipping, ultimately resulting in the rupture of the material at the point of maximum shear stresses. While the macroscopic deformation may simulate flexural buckling, it is important to
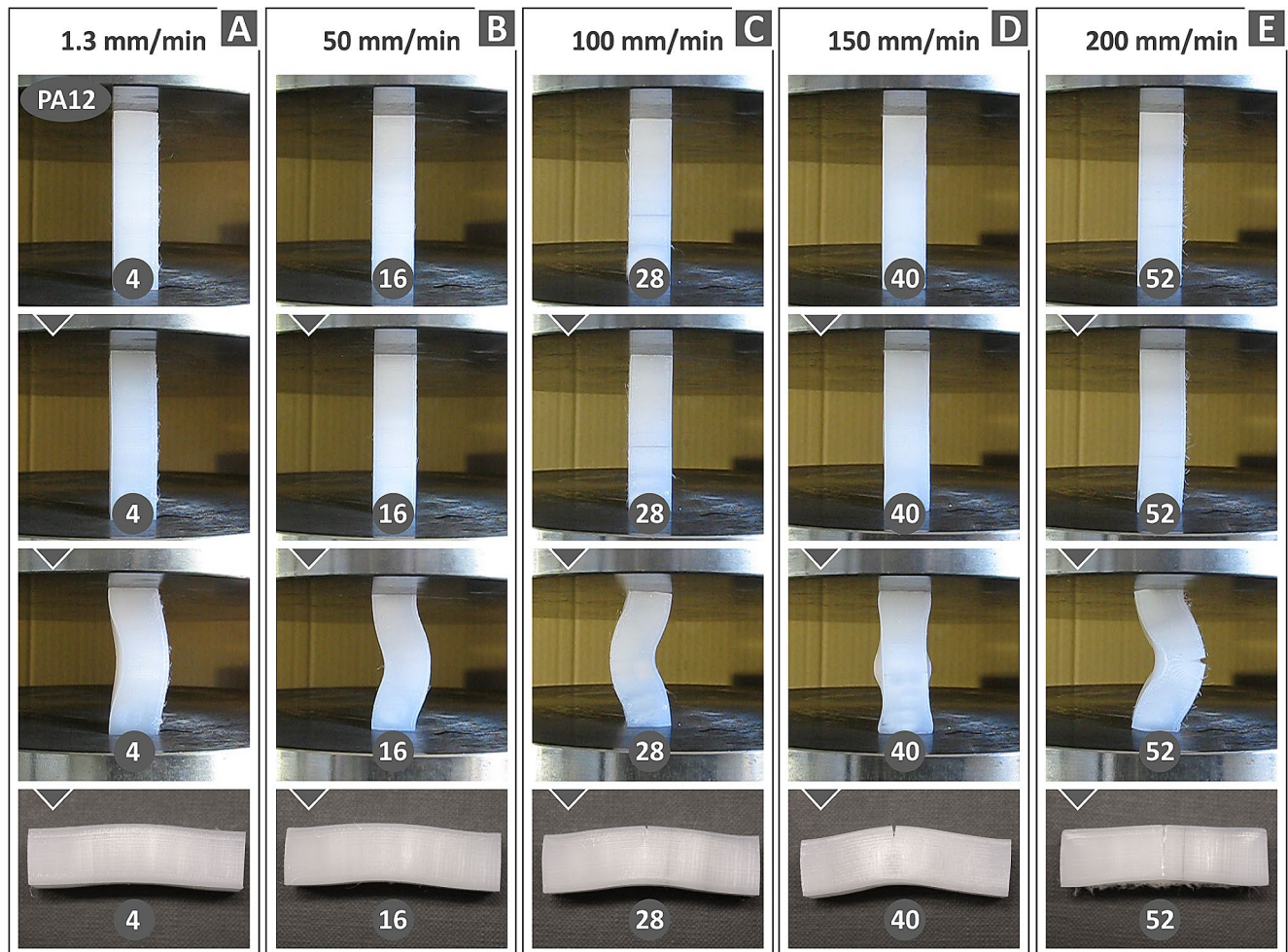
Fig. 12 PA12 polymer specimens' deformation at different compression speeds, a) at 1.3 mm/min, (b) at 50 mm/min, (c) at 100 mm/min, (d) at 150 mm/min, and (e) at 200 mm/min

note that the fundamental cause is not elastic deformation typical in bulk materials but rather the shear failure of the structure. Consequently, the material fails at the maximum compressive load, leading to the inference that this load signifies the ultimate compressive strength of the specimen. The compression test was terminated upon reaching an axial specimen deformation of 10 mm, rather than waiting for the formation of cracks or the material to fracture. The observed lower material toughness of the PP is attributed to its surface area under the stress-strain curve being the smallest in comparison to the other materials tested.

Especially for the PLA polymer, the overhangs formed during the axial compression of the PLA specimens are a result of shear bands sliding. The exclusive appearance of overhangs in PLA observed consistently across all tests at different strain rates, suggests a pronounced shear failure tendency in this material. This may be attributed to poor filament bonding which leads to a tendency for the creation of shear bands. This poor filament bonding can be a quality of the specific PLA grade examined or attributed to the 3D printing settings used. For example, a minor increase in the nozzle temperature could lead to a less viscous filament during the extrusion process, which may contribute to a better bonding between the strands. This requires additional tests to be defined on the specific PLA grade, which was not within the scope of the study.

The behavior of materials under varying strain rates is a crucial factor in understanding how they react in dynamic loading scenarios. In components constructed using Additive Manufacturing (AM) technology, this aspect becomes even more crucial. This is because the 3D printing parameters used in the construction process introduce a form of anisotropic behavior, which has a substantial impact on the mechanical characteristics of the resulting 3D printed components. This phenomenon primarily arises from the quality achieved in the fusion of the structural elements during the build and the bonding
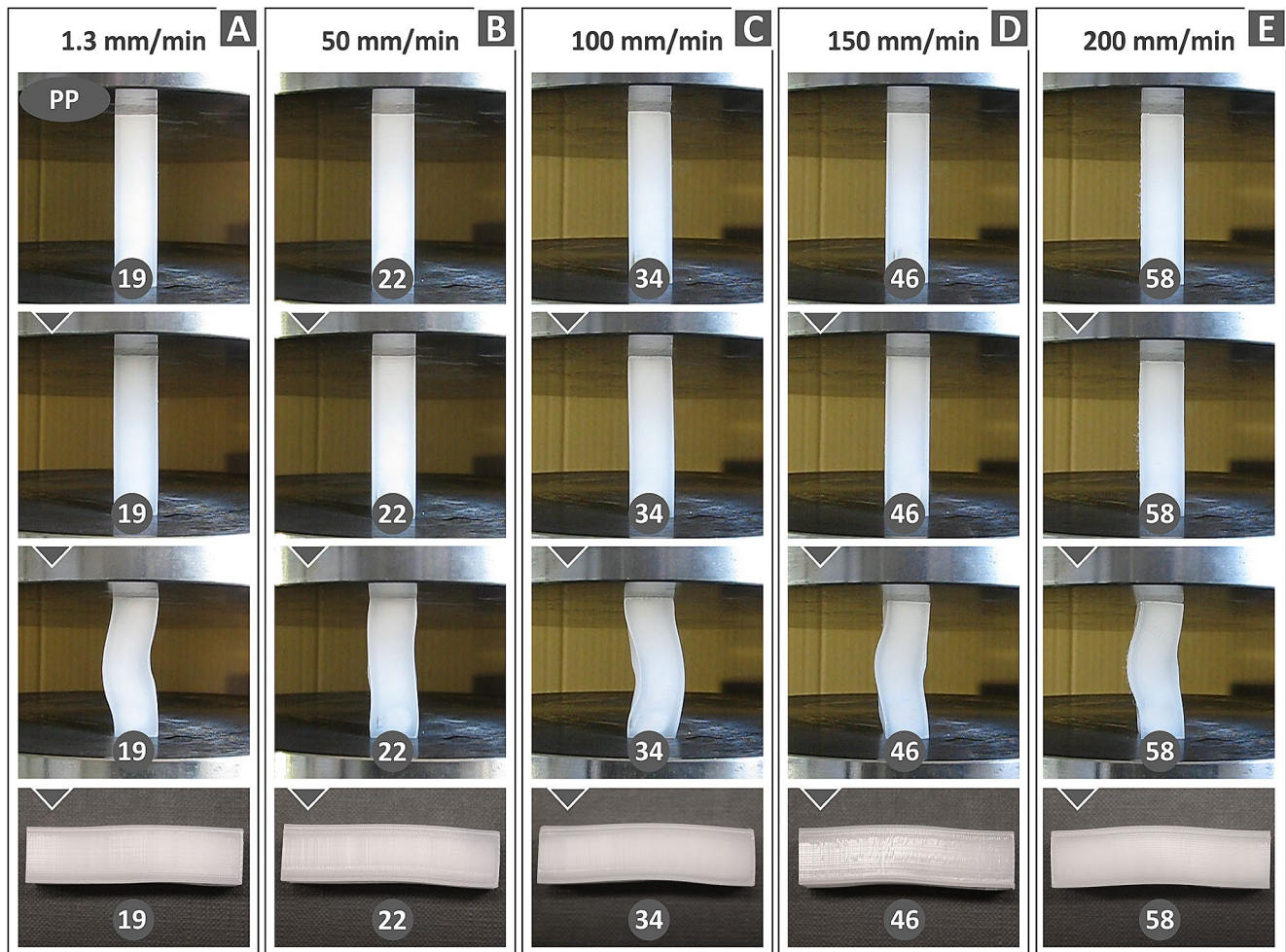
Fig. 13 PP polymer specimens' deformation at different compression speeds, a) at 1.3 mm/min, (b) at 50 mm/min, (c) at 100 mm/min, (d) at 150 mm/min, and (e) at 200 mm/min

that occurs both within and between layers throughout the manufacturing process of these components [84].

Herein, the importance of the compressive loadings and the investigation of the polymeric materials was justified and reported. The differences in the response of the polymeric materials further justify the merit of such investigations, especially in 3D printed parts, evaluating also the effect of the process on the performance of parts built with it. Since the strain rate hardening phenomena were confirmed in all four different 3D printed polymeric parts investigated, the results can be exploited in the design of the parts. The parts can withstand higher engineering loads in cases in which the operating conditions indicate higher strain rates for the applied engineering loads. The increase in the compressive strength reached 25% for most of the polymers. The yield stress had a similar increase and response to the compressive strength in all four polymers. The modulus of elasticity also increased, i.e., with the increase of the strain rate the

polymers showed a stiffer response (lower deformation for the same applied engineering load). The increase in the modulus of elasticity varied from about 10% (PLA) to almost 30% (PP) between the four polymers studied. As a result, constructions can be designed to be more lightweight, the safety factors can be increased, and parts can be stiffer and with decreased dimensions.

Comparing the findings herein with the literature, it can be concluded that they are in good agreement, with a similar response reported for the PLA polymer in 3D printed parts. A similar pattern for the increase of the strength is reported and the strength values are rather close [85, 86]. Similar strength values are reported for the ABS polymer for both 3D printed [87] and non-3D printed parts [88, 89]. For the 3D printed parts [87], the deformation of the samples as shown under the microscope, evolves in a similar manner to the samples in the current study. Corresponding comparison results are derived for the 3D printed polyamide and polyamide composites [90–92],
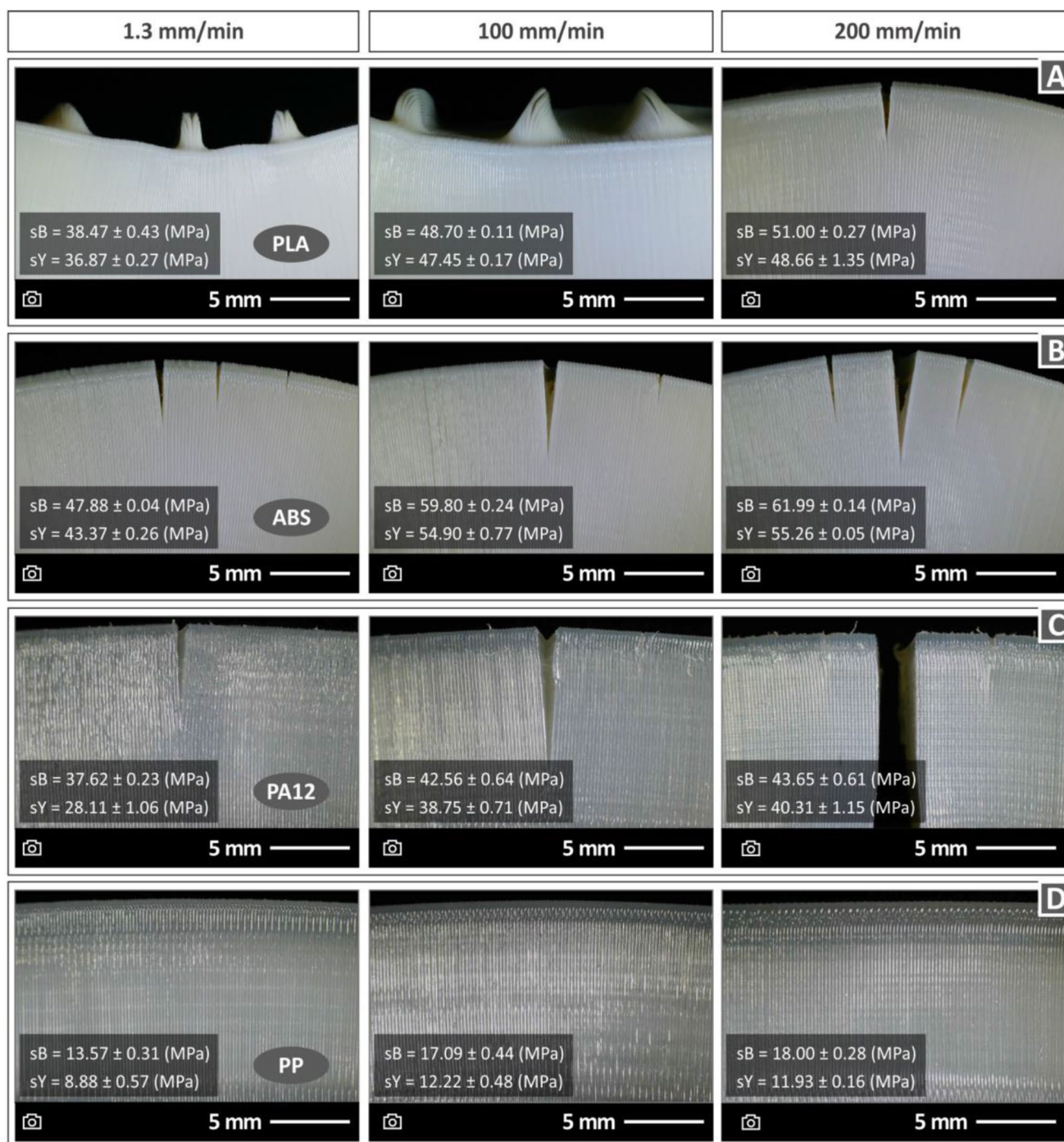
Fig. 14 Morphological characteristics at 1.3, 100, and 200 mm/min compression speeds for (a) PLA, (b) ABS, (c) PA12, and (d) PP polymer samples

bulk [93, 94], and 3D printed [95] PP polymer or its composites. The difference between the values reported in the different studies can be attributed to various parameters, such as the different grades of the polymers, the different 3D printing settings, etc. Still, similar patterns are observed with the increase of the strain rates in the tests and the values on the studies on 3D printed samples are close. Still, none of the aforementioned studies is similar to the current study parts tested in the range of strain rates applied herein. Most of the studies focus on composites tested with dynamic loads and some of the works are not on 3D printed samples, or samples 3D printed with other than the MEX 3D printed process were tested. Finally, the compression toughness and the strain rate sensitivity

index were not assessed in most of these works. Hence, the evaluation of the literature verifies the reliability of the findings presented herein and further supports their merit.

Conclusions

In conclusion, this study focused on conducting a compression sensitivity analysis of four widely utilized polymers in the context of the FFF additive manufacturing technique. The compression ratio emerges as a factor intertwined with dynamic loadings, which find application across diverse structural domains. Presently, limited research exists on investigating the impact of compression ratio on FFF 3D printed specimens. Notably, for the PLA, ABS, PA12, and PP polymers, no similar study has been introduced so far. Throughout the filament preparation and extrusion phases, all procedural steps were diligently followed to ensure the quality of the filaments. For the fabrication of specimens, the 3D printing parameters were configured to attain optimal quality, incorporating solid infill. The computations concerning compression strain show the behavior of all four polymers under varying compression speeds. Moreover, the derivation of the sensitivity index ("m") and the analysis of durability under distinct compression conditions can be used as useful design parameters for forthcoming research studies. As expected, the compression strength of all four polymers increased with the increase of the strain rate. ABS developed the highest compression strength and modulus of elasticity among the four polymers and the PP had the lowest compression properties. PP, at the same time, had higher strain rate sensitivity than the other three polymers, showing that it is higher affected by the change in the strain rate than the remaining polymers. The reported results provide useful information for the design of parts with these specific polymers and can be used for the optimization of the design, according to the working conditions in each case. In future work, additional polymers can be evaluated, and the range of the applied test speeds can be widened, by increasing the maximum test speed of the current research.

Data Availability The raw data presented in this study are available on request from the corresponding author.

Declarations

References

1. Wong KV, Hernandez A (2012) A review of Additive, Manufacturing. ISRN Mech Eng 2012:1–10. https://doi.org/10.5402/2012/208760
2. Vidakis N, Petousis M, Tzounis L, Velidakis E, Mountakis N, Grammatikos SA (2021) Polyamide 12/Multiwalled Carbon Nanotube and Carbon Black nanocomposites manufactured by 3D Printing Fused Filament Fabrication: a comparison of the Electrical, Thermoelectric, and Mechanical properties. 7:38. https://doi.org/10.3390/c7020038
3. Savolainen J, Collan M (2020) How additive Manufacturing Technology Changes Business models? – review of literature. Additive Manuf 32:101070. https://doi.org/10.1016/j.addma.2020.101070
4. Challagulla NV, Rohatgi V, Sharma D, Kumar R (2020) Recent developments of nanomaterial applications in additive manufacturing: a brief review. Curr Opin Chem Eng 28:75–82. https://doi.org/10.1016/j.coche.2020.03.003
5. Picard M, Mohanty AK, Misra M (2020) Recent advances in additive manufacturing of engineering thermoplastics: challenges and opportunities. RSC Adv 10:36058–36089
6. Chen P, Wang H, Su J, Tian Y, Wen S, Su B, Yang C, Chen B, Zhou K, Yan C, Shi Y (2022) Recent advances on high-performance polyaryletherketone materials for Additive Manufacturing. Adv Mater 34:2200750. https://doi.org/10.1002/adma.202200750
7. Ahmadifar M, Benfriha K, Shirinbayan M, Tcharkhtchi A (2021) Additive manufacturing of polymer-based composites using fused filament fabrication (FFF): a review. Appl Compos Mater 28:1335–1380
8. Saleh Alghamdi S, John S, Roy Choudhury N, Dutta NK (2021) Additive Manufacturing of Polymer materials: Progress, Promise and challenges. Polymers 13:753. https://doi.org/10.3390/polym13050753
9. Yap YL, Sing SL, Yeong WY (2020) A review of 3D printing processes and materials for soft robotics. RPJ 26:1345–1361. https://doi.org/10.1108/RPJ-11-2019-0302
10. Saluja A, Xie J, Fayazbakhsh K (2020) A closed-loop in-process warping detection system for fused filament fabrication using convolutional neural networks. J Manuf Process 58:407–415. https://doi.org/10.1016/j.jmapro.2020.08.036
11. Thrimurthulu K, Pandey PM, Venkata N, Reddy (2004) Optimum part deposition orientation in fused deposition modeling. Int J Mach Tools Manuf 44:585–594. https://doi.org/10.1016/j.ijmachtools.2003.12.004

12. Abeykoon C, Sri-Amphorn P, Fernando A (2020) Optimization of fused deposition modeling parameters for improved PLA and ABS 3D printed structures. Int J Lightweight Mater Manuf 3:284–297. https://doi.org/10.1016/j.ijlmm.2020.03.003

13. Zander NE, Gillan M, Burckhard Z, Gardea F (2019) Recycled polypropylene blends as novel 3D printing materials. Additive Manuf 25:122–130. https://doi.org/10.1016/j.addma.2018.11.009

14. Kam M, İpekçi A, Şengül Ö (2023) Investigation of the effect of FDM process parameters on mechanical properties of 3D printed PA12 samples using Taguchi method. J Thermoplast Compos Mater 36:307–325. https://doi.org/10.1177/08927057211006459

15. Dong M, Zhang S, Gao D, Chou B (2019) The study on polypropylene applied in fused deposition modeling. AIP Conf Proc 2065:030059. https://doi.org/10.1063/1.5088317

16. Raj A, Prashantha K, Samuel C (2020) Compatibility in biobased poly(L-lactide)/polyamide binary blends: from melt-state interfacial tensions to (thermo)mechanical properties. J Appl Polym Sci 137:48440. https://doi.org/10.1002/app.48440

17. Cunningham MF, Campbell JD, Fu Z, Bohling J, Leroux JG, Mabee W, Robert T (2019) Future green chemistry and sustainability needs in polymeric coatings. Green Chem 21:4919–4926. https://doi.org/10.1039/C9GC02462J

18. Wang L, Gramlich WM, Gardner DJ (2017) Improving the impact strength of poly(lactic acid) (PLA) in fused layer modeling (FLM). Polymer 114:242–248. https://doi.org/10.1016/j.polymer.2017.03.011

19. Buj-Corral I, Sanz-Fraile H, Ulldemolins A, Tejo-Otero A, Domínguez-Fernández A, Almendros I, Otero J (2022) Characterization of 3D printed Metal-PLA Composite scaffolds for Biomedical Applications. Polymers 14:2754. https://doi.org/10.3390/polym14132754

20. Serra T, Planell JA, Navarro M (2013) High-resolution PLA-based composite scaffolds via 3-D printing technology. Acta Biomater 9:5521–5530. https://doi.org/10.1016/j.actbio.2012.10.041

21. Alam F, Shukla VR, Varadarajan KM, Kumar S (2020) Microarchitected 3D printed polylactic acid (PLA) nanocomposite scaffolds for biomedical applications. J Mech Behav Biomed Mater 103:103576. https://doi.org/10.1016/j.jmbbm.2019.103576

22. Abifarin JK, Prakash C, Singh S (2022) Optimization and significance of fabrication parameters on the mechanical properties of 3D printed Chitosan/PLA scaffold. Mater Today: Proc 50:2018–2025. https://doi.org/10.1016/j.matpr.2021.09.386

23. Kechagias JD, Vidakis N, Petousis M, Mountakis N (2023) A multi-parametric process evaluation of the mechanical response of PLA in FFF 3D printing. Mater Manuf Processes 38:941–953. https://doi.org/10.1080/10426914.2022.2089895

24. Vidakis N, David C, Petousis M, Sagris D, Mountakis N, Moutsopoulou A (2022) The effect of six key process control parameters on the surface roughness, dimensional accuracy, and porosity in material extrusion 3D printing of polylactic acid: prediction models and optimization supported by robust design analysis. Adv Industrial Manuf Eng 5:100104. https://doi.org/10.1016/j.aime.2022.100104

25. Subramaniam SR, Samykano M, Selvamani SK, Ngui WK, Kadirgama K, Sudhakar K (2019) M.S. Idris, 3D printing: Overview of PLA progress, in: Kuantan, Malaysia,: p. 020015. https://doi.org/10.1063/1.5085958

26. Chacón JM, Caminero MA, García-Plaza E, Núñez PJ (2017) Additive manufacturing of PLA structures using fused deposition modelling: Effect of process parameters on mechanical properties and their optimal selection. Mater Design 124:143–157. https://doi.org/10.1016/j.matdes.2017.03.065

27. Gunasekaran KN, Aravinth V, Muthu Kumaran CB, Madhankumar K, Kumar SP (2021) Investigation of mechanical properties of PLA printed materials under varying infill density. Mater Today: Proc 45:1849–1856. https://doi.org/10.1016/j.matpr.2020.09.041

28. Petousis M, Moutsopoulou A, Korlos A, Papadakis V, Mountakis N, Tsikritzis D, Ntintakis I, Vidakis N (2023) The Effect of Nano Zirconium Dioxide (ZrO2)-Optimized content in Polyamide 12 (PA12) and polylactic acid (PLA) matrices on their Thermomechanical response in 3D Printing. Nanomaterials 13:1906. https://doi.org/10.3390/nano13131906

29. Petousis M, Vidakis N, Mountakis N, Karapidakis E, Moutsopoulou A (2023) Functionality Versus sustainability for PLA in MEX 3D Printing: the impact of generic process control factors on Flexural Response and Energy Efficiency. Polymers 15:1232. https://doi.org/10.3390/polym15051232

30. Ho K-LG, Pometto AL, Gadea-Rivas A, Briceño JA, Rojas A (1999) Degradation of Polylactic Acid (PLA) Plastic in Costa Rican Soil and Iowa State University Compost Rows. J Environ Polym Degrad 7:173–177. https://doi.org/10.1023/A:1022874530586

31. Swetha TA, Bora A, Mohanrasu K, Balaji P, Raja R, Ponnuchamy K, Muthusamy G, Arun A (2023) A comprehensive review on polylactic acid (PLA) – synthesis, processing and application in food packaging. Int J Biol Macromol 234:123715. https://doi.org/10.1016/j.ijbiomac.2023.123715

32. Petousis M, Vidakis N, Mountakis N, Papadakis V, Kanellopoulou S, Gaganatsiou A, Stefanoudakis N, Kechagias J (2022) Multifunctional material extrusion 3D-Printed Antibacterial Polylactic Acid (PLA) with binary inclusions: the Effect of Cuprous Oxide and Cellulose nanofibers. Fibers 10:52. https://doi.org/10.3390/fib10060052

33. Pakkanen J, Manfredi D, Minetola P, Iuliano L (2017) About the Use of recycled or biodegradable filaments for sustainability of 3D Printing. In: Campana G, Howlett RJ, Setchi R, Cimatti B (eds) Sustainable design and Manufacturing 2017. Springer International Publishing, Cham, pp 776–785

34. Bakhtiari H, Aamir M, Tolouei-Rad M (2023) Effect of 3D Printing parameters on the fatigue properties of Parts manufactured by Fused Filament Fabrication: a review. Appl Sci 13:904. https://doi.org/10.3390/app13020904

35. Vidakis N, David C, Petousis M, Sagris D, Mountakis N (2023) Optimization of key quality indicators in material extrusion 3D printing of acrylonitrile butadiene styrene: the impact of critical process control parameters on the surface roughness, dimensional accuracy, and porosity. Mater Today Commun 34:105171. https://doi.org/10.1016/j.mtcomm.2022.105171

36. Li D, Wang S (2021) Acrylonitrile–Butadiene–Styrene (ABS) Polymers, in: Kirk-Othmer Encyclopedia of Chemical Technology,: pp. 1–27. https://doi.org/10.1002/0471238961.01021911211209.a01.pub3

37. Ramezani Dana H, Barbe F, Delbreilh L, Azzouna MB, Guillet A, Breteau T (2019) Polymer additive manufacturing of ABS structure: influence of printing direction on mechanical properties. J Manuf Process 44:288–298. https://doi.org/10.1016/j.jmapro.2019.06.015

38. Ahn S, Montero M, Odell D, Roundy S, Wright PK (2002) Anisotropic material properties of fused deposition modeling ABS. Rapid Prototyp J 8:248–257. https://doi.org/10.1108/13552540210441166

39. Graziano A, Jaffer S, Sain M (2019) Review on modification strategies of polyethylene/polypropylene immiscible thermoplastic polymer blends for enhancing their mechanical behavior. J Elastomers Plast 51:291–336. https://doi.org/10.1177/0095244318783806

40. Hisham A, Maddah, Review (2016) Am J Polym Sci 6:1–11. https://doi.org/10.5923/j.ajps.20160601.01

41. Winter K, Wilfert J, Häupler B, Erlmann J, Altstädt V (2022) Large scale 3D Printing: influence of Fillers on Warp Deformation and on Mechanical properties of printed Polypropylene

Components. Macromol Mater Eng 307:2100528. https://doi.org/10.1002/mame.202100528

42. Shulga E, Karamov R, Sergeichev IS, Konev SD, Shurygina LI, Akhatov IS, Shandakov SD (2020) Nasibulin, Fused Filament fabricated polypropylene Composite Reinforced by Aligned Glass fibers. Materials 13. https://doi.org/10.3390/ma13163442

43. Yang H-S, Gardner DJ, Nader JW Characteristic impact resistance model analysis of cellulose nanofibril-filled polypropylene composites. Compos Part A: Appl Sci Manufac 42 (2011) 2028–2035. https://doi.org/10.1016/j.compositesa.2011.09.009

44. Barkoula N-M, Alcock B, Cabrera NO, Peijs T (2008) Fatigue properties of highly oriented polypropylene Tapes and all-polypropylene composites. Polym Polym Compos 16:101–113. https://doi.org/10.1177/096739110801600203

45. Vidakis N, Petousis M, Mountakis N, Maravelakis E, Zaoutsos S, Kechagias JD (2022) Mechanical response assessment of antibacterial PA12/TiO2 3D printed parts: parameters optimization through artificial neural networks modeling. Int J Adv Manuf Technol 121:785–803. https://doi.org/10.1007/s00170-022-09376-w

46. Vidakis N, Petousis M, Kechagias JD (2022) Parameter effects and process modelling of polyamide 12 3D-printed parts strength and toughness. Mater Manuf Processes 37:1358–1369. https://doi.org/10.1080/10426914.2022.2030871

47. Zhu D, Ren Y, Liao G, Jiang S, Liu F, Guo J, Xu G (2017) Thermal and mechanical properties of polyamide 12/graphene nanoplatelets nanocomposites and parts fabricated by fused deposition modeling: ARTICLE. J Appl Polym Sci 134:45332. https://doi.org/10.1002/app.45332

48. Hofland EC, Baran I, Wismeijer DA (2017) Correlation of process parameters with Mechanical properties of Laser Sintered PA12 Parts. Adv Mater Sci Eng 2017:4953173. https://doi.org/10.1155/2017/4953173

49. Alzyod H, Ficzere P (2023) Optimizing fused filament fabrication process parameters for quality enhancement of PA12 parts using numerical modeling and taguchi method. Heliyon 9:e14445. https://doi.org/10.1016/j.heliyon.2023.e14445

50. Tymrak BM, Kreiger M, Pearce JM (2014) Mechanical properties of components fabricated with open-source 3-D printers under realistic environmental conditions. Mater Design 58:242–246. https://doi.org/10.1016/j.matdes.2014.02.038

51. Lanzotti A, Grasso M, Staiano G, Martorelli M (2015) The impact of process parameters on mechanical properties of parts fabricated in PLA with an open-source 3-D printer. Rapid Prototyp J 21:604–617. https://doi.org/10.1108/RPJ-09-2014-0135

52. Enhancing the Structural Performance of Additively Manufactured Objects Through Build (2023) Orientation Optimization| J. Mech. Des.| ASME Digital Collection, (n.d.). https://asmedigitalcollection.asme.org/mechanicaldesign/article-abstract/137/11/111410/474824/Enhancing-the-Structural-Performance-of-Additively?redirectedFrom=fulltext

53. Durgun I, Ertan R (2014) Experimental investigation of FDM process for improvement of mechanical properties and production cost. Rapid Prototyp J 20:228–235. https://doi.org/10.1108/RPJ-10-2012-0091

54. Vidakis N, Petousis M, Tzounis L, Maniadi A, Velidakis E, Mountakis N, Papageorgiou D, Liebscher M, Mechtcherine V (2020) Sustainable Additive Manufacturing: mechanical response of polypropylene over multiple recycling processes. Sustainability 13:159. https://doi.org/10.3390/su13010159

55. Li JH, Huang XD, Durandet Y, Ruan D (2021) A review of the mechanical properties of additively manufactured fiber reinforced composites, IOP conf. Ser: Mater Sci Eng 1067:012105. https://doi.org/10.1088/1757-899X/1067/1/012105

56. Ngo TD, Kashani A, Imbalzano G, Nguyen KTQ, Hui D (2018) Additive manufacturing (3D printing): a review of materials, methods, applications and challenges. Compos Part B: Eng 143:172–196. https://doi.org/10.1016/j.compositesb.2018.02.012

57. Tzounis L, Bangeas PI, Exadaktylos A, Petousis M, Vidakis N (2020) Three-dimensional printed polylactic acid (PLA) Surgical retractors with Sonochemically immobilized silver nanoparticles: the next generation of low-cost antimicrobial surgery equipment. Nanomaterials 10:985. https://doi.org/10.3390/nano10050985

58. Vidakis N, Petousis M, Korlos A, Velidakis E, Mountakis N, Charou C, Myftari A (2021) Strain rate sensitivity of polycarbonate and thermoplastic polyurethane for various 3D Printing temperatures and Layer Heights. Polymers 13:2752. https://doi.org/10.3390/polym13162752

59. Rezgui F, Swistek M, Hiver JM, G'Sell C, Sadoun T (2005) Deformation and damage upon stretching of degradable polymers (PLA and PCL). Polymer 46:7370–7385. https://doi.org/10.1016/j.polymer.2005.03.116

60. Ching ECY, Li RKY, Mai Y-W (2000) Effects of gauge length and strain rate on fracture toughness of polyethylene terephthalate glycol (PETG) film using the essential work of fracture analysis. Polym Eng Sci 40:310–319. https://doi.org/10.1002/pen.11164

61. Shan G-F, Yang W, Yang M, Xie B, Feng J, Fu Q (2007) Effect of temperature and strain rate on the tensile deformation of polyamide 6. Polymer 48:2958–2968. https://doi.org/10.1016/j.polymer.2007.03.013

62. Demir S, Yüksel C (2023) Evaluation of effect and optimizing of process parameters for fused deposition modeling parts on tensile properties via Taguchi method. RPJ 29:720–730. https://doi.org/10.1108/RPJ-06-2022-0201

63. Heidari-Rarani M, Ezati N, Sadeghi P, Badrossamay M (2022) Optimization of FDM process parameters for tensile properties of polylactic acid specimens using Taguchi design of experiment method. J Thermoplast Compos Mater 35:2435–2452. https://doi.org/10.1177/0892705720964560

64. Raju R, Varma MMMK, Kumar P, Baghel (2022) Optimization of process parameters for 3D printing process using Taguchi based grey approach, Materials Today: Proceedings 68 1515–1520. https://doi.org/10.1016/j.matpr.2022.07.163

65. Teharia R, Singari RM, Kumar H (2022) Optimization of process variables for additive manufactured PLA based tensile specimen using taguchi design and artificial neural network (ANN) technique. Mater Today: Proc 56:3426–3432. https://doi.org/10.1016/j.matpr.2021.10.376

66. Teng HM, Fan SK, Jiang CH, Yang QW, Liu FH, Tsao CC (2022) Study on the printing quality of fused deposition modeling using Taguchi method. J Phys: Conf Ser 2345:012014. https://doi.org/10.1088/1742-6596/2345/1/012014

67. Silva FS (2005) The importance of compressive stresses on fatigue crack propagation rate. Int J Fatigue 27:1441–1452. https://doi.org/10.1016/j.ijfatigue.2005.07.003

68. Hatta H, Goto K, Aoki T (2005) Strengths of C/C composites under tensile, shear, and compressive loading: role of interfacial shear strength. Compos Sci Technol 65:2550–2562. https://doi.org/10.1016/j.compscitech.2005.07.012

69. Vidakis N, Petousis M, Karapidakis E, Mountakis N, David C, Sagris D (2023) Energy consumption versus strength in MEX 3D printing of polylactic acid. Adv Industrial Manuf Eng 100119. https://doi.org/10.1016/j.aime.2023.100119

70. Dasari A, Misra RDK (2003) On the strain rate sensitivity of high density polyethylene and polypropylenes. Mater Sci Engineering: A 358:356–371. https://doi.org/10.1016/S0921-5093(03)00330-7

71. Vairis A, Petousis M, Vidakis N, Savvakis K (2016) On the strain rate sensitivity of Abs and abs plus fused deposition modeling parts. J Mater Eng Perform 25. https://doi.org/10.1007/s11665-016-2198-x

72. Vidakis N, Petousis M, Velidakis E, Liebscher M, Mechtcherine V, Tzounis L (2020) On the strain rate sensitivity of fused filament fabrication (FFF) processed PLA, ABS, PETG, PA6, and PP thermoplastic polymers. Polymers 12. https://doi.org/10.3390/polym12122924

73. Ntintakis I, Stavroulakis GE (2022) Infill microstructures for Additive Manufacturing. Appl Sci 12:7386. https://doi.org/10.3390/app12157386

74. Petousis M, Ntintakis I, David C, Sagris D, Nasikas NK, Korlos A, Moutsopoulou A, Vidakis N (2023) A coherent Assessment of the compressive strain rate response of PC, PETG, PMMA, and TPU thermoplastics in MEX Additive Manufacturing. Polymers 15. https://doi.org/10.3390/polym15193926

75. Selvamani SK, Rajan K, Samykano M, Kumar RR, Kadirgama K, Mohan RV (2022) Investigation of tensile properties of PLA–brass composite using FDM. Progress Additive Manuf 7:839–851. https://doi.org/10.1007/s40964-021-00255-6

76. Barba D, Arias A, Garcia-Gonzalez D (2020) Temperature and strain rate dependences on hardening and softening behaviours in semi-crystalline polymers: application to PEEK. Int J Solids Struct 182–183:205–217. https://doi.org/10.1016/j.ijsolstr.2019.08.021

77. Ahmed A, Zillur Rahman M, Ou Y, Liu S, Mobasher B, Guo S, Zhu D (2021) A review on the tensile behavior of fiber-reinforced polymer composites under varying strain rates and temperatures. Constr Build Mater 294:123565–123565. https://doi.org/10.1016/j.conbuildmat.2021.123565

78. Merlette TC, Hem J, Crauste-Thibierge C, Ciliberto S, Clément F, Sotta P, Long DR (2023) Theory of plasticity and strain hardening of glassy polymers. Macromolecules 56:6510–6526. https://doi.org/10.1021/acs.macromol.3c00526

79. Herbert KM, Fowler HE, McCracken JM, Schlafmann KR, Koch JA, White TJ (2022) Synthesis and alignment of liquid crystalline elastomers. Nat Reviews Mater 7:23–38. https://doi.org/10.1038/s41578-021-00359-z

80. Ding Z, Liu D, Zhao K, Han Y (2021) Optimizing morphology to Trade off Charge Transport and Mechanical Properties of Stretchable Conjugated Polymer Films. Macromolecules 54:3907–3926. https://doi.org/10.1021/acs.macromol.1c00268

81. Petersen SR, Prydderch H, Worch JC, Stubbs CJ, Wang Z, Yu J, Arno MC, Dobrynin AV, Becker ML, Dove AP (2022) Ultra-tough elastomers from Stereochemistry-Directed Hydrogen Bonding in Isosorbide-based polymers. Angew Chem Int Ed 61:e202115904–e202115904. https://doi.org/10.1002/anie.202115904

82. Sanoja GE, Morelle XP, Comtet J, Yeh CJ, Ciccotti M, Creton C Why is mechanical fatigue different from toughness in elastomers? The role of damage by polymer chain scission, Science Advances 7 (n.d.) eabg9410. https://doi.org/10.1126/sciadv.abg9410

83. Zhong H, Zhang M (2021) Effect of recycled tyre polymer fibre on engineering properties of sustainable strain hardening geopolymer composites. Cem Concr Compos 122:104167–104167. https://doi.org/10.1016/j.cemconcomp.2021.104167

84. Vidakis N, Petousis M, Vairis A, Savvakis K, Maniadi A (2017) On the compressive behavior of an FDM Steward platform part. J Comput Des Eng 4:339–346. https://doi.org/10.1016/j.jcde.2017.06.001

85. Priyanka G, Saideep C, Tadepalli T (2022) Dynamic characterization of Additively Manufactured Polylactide (PLA). Proc Institution Mech Eng Part L: J Materials: Des Appl 236:963–976. https://doi.org/10.1177/14644207211065149

86. Foroughi AH, Valeri C, Jiang D, Ning F, Razavi M, Razavi MJ (2023) Understanding compressive viscoelastic properties of additively manufactured PLA for bone-mimetic scaffold design. Med Eng Phys 114:103972. https://doi.org/10.1016/j.medengphy.2023.103972

87. Jami H, Masood SH, Song WQ (2018) Dynamic stress-strain compressive behaviour of FDM made ABS and PC parts under high strain rates, IOP Conference Series: Materials Science and Engineering 377 012153. https://doi.org/10.1088/1757-899X/377/1/012153

88. Wang H, Zhang Y, Huang Z, Gao H, Zhang Y, Gao X, Zhou H (2016) Experimental and modeling study of the compressive behavior of PC/ABS at low, moderate and high strain rates. Polym Test 56:115–123. https://doi.org/10.1016/j.polymertesting.2016.09.027

89. Dundar MA, Dhaliwal GS, Ayorinde E, Al-Zubi M (2021) Tensile, compression, and flexural characteristics of acrylonitrile–butadiene–styrene at low strain rates: experimental and numerical investigation. Polym Polym Compos 29:331–342. https://doi.org/10.1177/0967391120916619

90. Zeybek MK, Güden M, Taşdemirci A (2023) The effect of strain rate on the Compression Behavior of Additively Manufactured Short Carbon Fiber-Reinforced Polyamide composites with different Layer Heights, Infill patterns, and built angles. J Mater Eng Perform. https://doi.org/10.1007/s11665-023-07918-1

91. Zheng X, Meng J, Liu Y (2022) Strain Rate Dependence of Compressive Mechanical Properties of Polyamide and its Composite fabricated using selective laser sintering under saturated-water conditions. Micromachines 13. https://doi.org/10.3390/mi13071041

92. Wang K, Xie G, Xiang J, Li T, Peng Y, Wang J, Zhang H (2022) Materials selection of 3D printed polyamide-based composites at different strain rates: a case study of automobile front bumpers. J Manuf Process 84:1449–1462. https://doi.org/10.1016/j.jmapro.2022.11.024

93. Okereke MI, Buckley CP, Siviour CR (2012) Compression of polypropylene across a wide range of strain rates. Mech Time-Dependent Mater 16:361–379. https://doi.org/10.1007/s11043-012-9167-z

94. Bouix R, Viot P, Lataillade J-L (2009) Polypropylene foam behaviour under dynamic loadings: strain rate, density and microstructure effects. Int J Impact Eng 36:329–342. https://doi.org/10.1016/j.ijimpeng.2007.11.007

95. Wang K, Cai R, Zhang Z, Liu J, Ahzi S, Peng Y, Rao Y (2021) Compressive behaviors of 3D printed polypropylene-based composites at low and high strain rates. Polym Test 103:107321. https://doi.org/10.1016/j.polymertesting.2021.107321